Photon strength function modelling, status and perspectives

Sophie Péru[1,2,*], *Stéphane* Goriely[3], and *Stéphane* Hilaire[1,2]

[1]CEA, DAM, DIF, F-91297 Arpajon, France
[2]Université Paris-Saclay, CEA, LMCE, 91680 Bruyères-le-Châtel, France
[3]Institut d'Astronomie et d'Astrophysique, Université Libre de Bruxelles, Campus de la Plaine CP 226, 1050 Brussels, Belgium

Abstract. The present contribution gives an overview of the photon strength function models developed to compensate for the lack of data for experimentally non-accessible nuclei. Phenomenological and microscopic approaches are presented in light of their respective strengths. Since the microscopic models included in the TALYS code are based on the quasi-particle random phase approximation (QRPA) method, the scope of application of this approach is presented. The QRPA-based strength functions, obtained using effective, covariant or Skyrme or Gogny interactions, reproduce the majority of experimental data with a variable level of precision which is briefly discussed. Some alternatives or updates to the gamma-ray strength functions based on QRPA methods are proposed. Returning to the definition of the photon strength function, particular attention is paid to the differences between the processes of photon absorption and the de-excitation of nuclei. As perspectives, preliminary theoretical results including probabilities of transition between excited states are presented.

1 Introduction

Among the nuclear quantities useful for nuclear physics applications, the photon strength function (PSF) is one for which many theoretical developments are now needed to complete databases and interpret new measurements. Even if it is not *stricto sensus* an observable, it can be inferred from experimental measurements and used as nuclear data. For this reason, the question of its definition is crucial for theorists who want to both reproduce it when it is "measured" and predict it for a nuclear system not accessible by any experimental setup. "*What is the photon strength function?*" remains a crucial question. We return here to the PSF initial definition and use, notably in nuclear reaction models. By improving our knowledge of the nuclear structure, we will present the evolution and the figures of merit of the different PSF models. To do this, a selection rule is chosen: will only be discussed here the models implemented, currently or in the near future, in the TALYS reaction code [1].

The following section provides some general information on nuclear spectroscopy and the overall characteristics of the PSF. Section 3 lists the PSF models currently included in TALYS, with emphasis on the QRPA approach and its alternatives. Section 4 presents recent improvements to the post-processing of QRPA outputs that allow for a microscopic and spontaneous low energy upbend in the γ-ray strength function. A summary and some perspectives are given in the last section of this contribution.

*e-mail: sophie.peru-desenfants@cea.fr

2 Historical definition of the Photon Strength Function

In the context of nuclear data required for reaction modeling, the PSF is equivalent to the γ- ray strength function. Although the latter is an important ingredient for reaction models, it is not an observable. A standardized and universal definition of PSF is crucial either to extract it from experiment or to evaluate it correctly from a theoretical point of view. So the question reads: *what is a γ-ray strength function?*

Many answers can be given, all are true. At first glance, a PSF is an entry in the TALYS code [1] which, combined with the nuclear level density, provides the electromagnetic deexcitation rates of the compound nucleus states to more bound states down to the ground state (GS); but it is also the ability of the nucleus in its GS to absorb a photon. This definition, which is centred on its numerical use, is nevertheless linked to a more academic definition: "for each excited state of a nucleus, the knowledge of a quantity proportional to the probability of absorbing or emitting a photon of a given energy". In fact, most of the characteristics of the nucleus are derived from spectroscopic information that can be used to determine the structure of finite nuclear systems. The previous question should therefore be reformulated: *why should a nucleus emit or absorb a photon?*

2.1 Main reasons for nuclear photon emission and absorption

A general knowledge of the nature of nuclear excitations is required to answer this question. Although each nucleus

is defined by its numbers of protons and neutrons (Z, N), it can be observed in different states depending on the arrangement of nucleons on their individual orbitals and according to collective movements such as a global vibration or rotation. Each of these states is characterized by its spin, its parity and also its excitation energy with respect to the ground state. These energies generally have discrete values up to a few MeV, although at high energy we observe a continuum due to a high level density. As written above, the first collective states can be either vibrational or rotational. Let us remind that the rotational bands are built by increasing the angular moment on so-called "band head" states: these may be vibrational excited states, K isomers, shape isomers or even the GS. If the observation of a rotation band is evidence of an intrinsic deformation of the nucleus studied, all nuclei, including spherical ones, can be excited in vibrational mode provided that they receive an appropriate amount of energy. Likewise, it is always possible for the excited nucleus to de-excite itself into another excited state including the GS via an electromagnetic transition of the required multipolarity. There is an exception in the case of monopole modes that do not require photon emission or absorption and therefore the probability of transition E0 is derived from measurements of conversion electrons or inelastic direct scattering of light nuclei. In fact, some rules of quantum mechanics limit the multipolarities and parities of these transitions according to the spin and parity of initial and final states. Thus, when the transition occurs from or to the GS of an even-even nucleus with spin and parity of 0^+, it is easy to associate the multipolarity of the transition with a multipolar mode of vibration of the same order, as shown in Fig. 1.

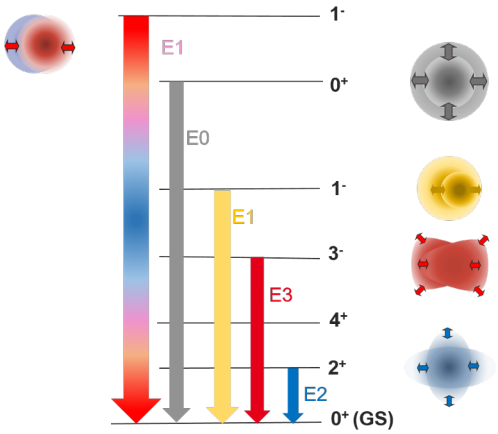

Figure 1. Example of multipole electromagnetic transitions between the even-even nucleus GS ($J^\pi = 0^+$) and excited states described as monopole (grey), dipole (yellow or rainbow), quadrupole (blue) and octupole (red) shape vibrations. The images on the right of the spectrum are schematic, they illustrate different isospin scalar (IS) modes, while the isospin vector (IV) dipole mode is represented on the left of the spectrum with a colour by isospin. For multipolarities $\lambda > 0$, a photon with an energy equal to the excitation energy can be emitted with a probability proportional to E_λ.

In this figure are shown schematic representations of electric modes, among them the monopole one (breathing mode) and quadrupole or octupole shape oscillations. Since protons and neutrons oscillate in phase for these three modes, they are defined as isospin-scalar modes, named isoscalar and referenced IS. For the dipole mode, both isospin (isovector or IV) vector modes and IS modes can be observed, especially for neutron-rich systems where low dipole excitations have been interpreted as the oscillation of a core against the neutron skin (yellow shape picture in Fig. 1). It is interesting to note that magnetic excitations are also generated for "unnatural parities" but induce currents inside the core rather than shape vibrations.

For a given value $\lambda > 0$, the transition probability between an initial state i and final one f with a photon of energy E_γ can be expressed as (see for example [2])

$$T_{fi}(X\lambda) = \frac{8\pi(\lambda+1)}{\hbar\lambda((2\lambda+1)!!)^2}\left(\frac{E_\gamma}{\hbar c}\right)^{2\lambda+1} B\left(X\lambda, I_i \rightarrow I_f\right) \quad (1)$$

where X=E stands for electric and M for magnetic modes of a given λ multipolarity and $B\left(X\lambda, I_i \rightarrow I_f\right)$ is the corresponding (electric or magnetic) reduced probability. From Eq. (1), it is obvious that dipole modes are favoured over higher multipolarities. In addition, the dipole electric mode is much more likely than the magnetic one : unit transformation from reduced matrix elements, expressed in μ_N^2 for magnetic and in e^2fm^2 for electric, to the transition probability T unit in s^{-1} induces a factor of one hundred between electric and magnetic probabilities since $1\mu_N^2 = 0.011057e^2fm^2$. These reasons are sufficient to understand that the PSF is mainly driven by the dipole modes and in particular by the IV Giant Dipole resonance (IVGDR). This may also explain why IVGDR is the first giant resonance (GR) that has been observed (for a history of the study of GRs, see [3]). Recall here that GRs are called giants because they exhaust most of the sum rule, i.e. they absorb the major part of the energy transferred to the nucleus. The photo-absorption cross section is mainly determined by the IVGDR contribution. We will see later that considering only photo-absorption is not enough to reproduce all experimental data but we keep this quantity as a starting point for any modeling.

2.2 General feature of the PSF

In the present sub-section, we indicate the hypothesis made in the oldest models and the systematic laws deduced from observation. More specifically, we present the overall characteristics of the known PSF from photo-absorption data and therefore IVGDR studies.

Assuming that the photo-absorption cross section is proportional to the electric dipole strength $S_{E1}(E_\gamma)$ multiplied by the energy of the absorbed photon E_γ, $S_{E1}(E_\gamma)$ can be expressed as a percentage of the Thomas-Reiche-Kuhn sum rule equal to 14.8 $NZ/A\ e^2fm^2$ MeV. We also know from the first measurements of GRs that the energy of the centroid is globally inversely proportional to the radius of the vibrating nuclei. Thus, laws in $A^{-1/3}$ have been

proposed for a systematic evaluation of the multipole GR centroid [4]. Because of the restoring force between protons and neutrons, the systematic law of the energy of the centroid of the IVGDR can be improved with the expression $E_{GDR,exp} = 31.2A^{-1/3} + 20.6A^{-1/6}$ MeV [3]. From recent microscopic calculations [5], one can extract an alternative law, namely $E_{GDR,th} = 41A^{-1/6}$ MeV. The centroid energy of PSF is found between 10 and 20 MeV for the whole nuclear chart. By increasing atomic masses, the PSF centroid energy decreases while its amplitude increases. For axially symmetrical deformed nuclei, the strength splits into two components; for triaxial shape [1] a division into three components is expected.

The reciprocity theorem is often used in many models that generate databases: the probabilities of absorption and emission are identical. This means that the definition of PSF is close to that of reduced transition probability. The latter gives both the probability of transition up and down but by reversing the initial and final spins in the calculation of the pre-factor (see for example p. 589 of Ref. [2]).

3 PSF models for reaction modeling

An important question for application is which theoretical approaches can provide reliable predictions for an appropriate use in reaction codes[2]. As an ingredient in the TALYS code, PSF models must be able to provide data for a large number of nuclei, i.e. all nuclei likely to exist and to be involved in nuclear processes. From a theoretical point of view, this means systematic calculations with model characterized by a minimum number of free parameters and the most robust theoretical foundation.

Learning from the global properties discussed above, most of the models providing such PSFs are analytical formulae, even if some microscopic models begin to emerge. Table 1 gives the list of current models implemented in TALYS, including their common name, their purely phenomenological character or microscopic foundations and the year of the associated reference publication.

The options 1-2-5 and 9 are clearly macroscopic models and will be briefly presented in the following subsection. The other models will be described in a separate sub-section as variants of the microscopic mean-field approach QRPA (for quasi-particle random phase approximation).

3.1 Phenomenological formulas, some successes and residual difficulties

The first formula of a PSF has been proposed more than 60 years ago by D. Brink in his PhD thesis and published a few years later by P. Axel [7]. In its formulation, the form of IVGDR is approximated by a Lorentzian function

[1] In the current framework, triaxial deformation means that nuclei are deformed without rotation symmetry around any axis, but where reflection symmetries relative to planes are possible. Parity is then associated with left-right symmetry.

[2] For more critical analysis and recommendations on the use of PSF reference databases, including experimental data, the reader can find information in Ref. [6]

Table 1. Current E1 PSF models included in the TALYS code [1] with their phenomenological/analytical (PA) or microscopic (MI) nature and the year of their publication inculded. T means temperature. Only models 8 and 9 provide E1 and M1 contributions consistently. See text for more details.

1	GLO	PA	1990
2	SLO	PA	1962
3	Skyrme-HFBCS+QRPA	MI	2002
4	Skyrme-HFB +QRPA	MI	2004
5	Hybrid	MI	1998
6	T-dependent Skyrme-HFB +QRPA	MI	2004
7	T-dependent RMF-HB +QRPA	MI	2012
8	Gogny-HFB +QRPA	MI	2018
9	SMLO	PA	2019
10	T-dependent BSk27-HFB +QRPA	MI	2021

for which the centroid energy is extracted from the above-mentioned systematic law. This formula leads to the standard Lorentzian (SLO) model. The other major hypothesis of this model is known as the Brink hypothesis: it assumes that the probability of absorption/emission is only related to the energy of the photon absorbed/emitted independently of the excitation energy (temperature) of the system. One of its main defect is that the resulting PSF is zero at the limit of small γ-ray energies. To overcome this, the generalized Lorentzian (GLO) model has been proposed [8]. It assumes that the width of the Lorentzian function varies with the photon energy and the temperature. The temperature (T) should be understood here as the excitation energy of the compound nucleus. Note that this dependence is the first violation of Brink's hypothesis. Along the same line, an hybrid model has been developed [9], this time to take into account the GLO description of the GDR region and the low-energy behaviour of the GDR as predicted within the Fermi liquid model of Kadmenskii et al. [10].

Let us stress that for axially deformed nuclei, the GLO, SLO and Hybrid PSFs are split into 2 Lorentzian functions. This split depends on the deformation parameter η and affects both the centroid energies and the widths of both components (labeled 1 and 2) by the simplest formulation [11]:

$$E_1 + 2E_2 = 3E_{spher.}, \quad E_2/E_1 = 0.911\eta + 0.089, \qquad (2)$$

The most recent analytical model is the Simplified Lorentzian Model (SMLO), which includes the E1 component as described by a generalized temperature-dependent formula [12] and an M1 component that takes into account magnetic states like spin-flip modes as well as scissors modes for deformed nuclei [13]. These magnetic properties are inspired by the D1M+QRPA model, a microscopic-based model which will be introduced in the next section. On top of that, M1 transitions occurring in decay processes only have been modelled to reproduce the so-called "upbend" observed in Oslo data [14, 15]. Such upbend properties have been inspired by the shell model (SM) predictions [16–18]. The presence of such a possible low-energy de-excitation M1 and its impact as an upbend on the PSF is the second violation of Brink's Hypothesis.

Although these models give accurate results for the nuclei on which they have been adjusted, it is difficult to trust the predictions of these purely phenomenological approaches when extrapolating for experimentally unreachable nuclei. Thus, more and more microscopic ingredients have been taken into account. It is now possible to go beyond simple Lorentzian or Hybrid approaches.

3.2 Common formalism for microscopic models: QRPA approaches

To take into account the greatest possible number and variety of states around the GDR, microscopic approaches have been used more intensively in recent decades for the description of the photon absorption. Since reciprocity between (emission) and excitation (absorption) is always fulfilled, the eligible models must be able to calculate either of the two processes for any (Z, N) system of interest. As seen in the Table 1, the microscopic models included in TALYS use a common approach, called QRPA. This theoretical framework is now presented in the following section dedicated to it.

3.2.1 The QRPA approach

Well known as an adequate approach to reproduce giant resonances of rigid nuclei, the QRPA approach presents a greater scope of applicability than is usually granted. A priori QRPA approaches describe high energy states as well as low energy ones with the same accuracy. Very powerful to account for collective vibrational states, this method also describes many other excited states that can be called "individual" because very few nucleons are involved. In addition, QRPA methods describe nuclear excitation states for all multipoles and both parities irrespective of the intrinsic deformation of the GS, as illustrated in Fig. 2 where not only monopole breathing mode but also quadrupole as well as dipole shapes are recovered by oscillation around a spherical shape.

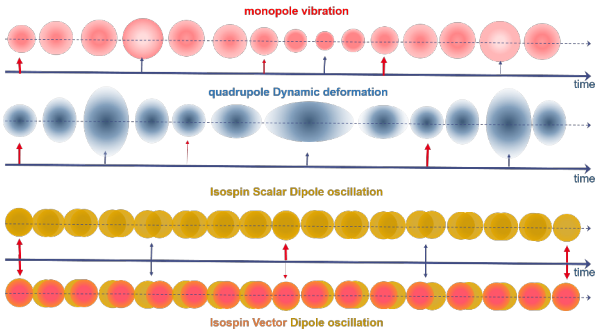

Figure 2. Example of vibrating shapes recovered by electromagnetic modes. Shapes are plotted as function of time. From the top to the bottom: monopole, quadrupole, IS-dipole, and IV dipole oscillations. Red arrows give the time of equilibrium shape and blue arrows the time of maximal shape deformations.

One can see from this figure that IV modes have a period twice as long as the IS. This is related to the IVGDR excitation energy which is found to be lower than the one of the ISGDR. However, even for deformed cores, no rotation mode is included in standard QRPA calculations. The other main hypothesis of this approach is the linear response assumption, i.e. the approximation of an harmonic potential in all directions. This means that, as soon as the system is in a minimum of a multidimensional energy surface (in deformation), one can extract locally the variation to the second order in all directions at once. With the knowledge of the definite positive second derivative, one can extrapolate the surface to the largest amplitudes and thus generate all vibrational states around the equilibrium state; this is illustrated by the two left schemes of Fig. 3.

In its standard formulation, solving the QRPA equation is equivalent to calculating an interaction matrix between all particle-hole (or two quasi-particles) excitations. Diagonalization provides eigenvalues, which are the excitation energies of the QRPA phonons, and the eigenvectors, named as QRPA amplitudes which are nothing less than phonon wave functions [19]. It is easy to calculate from these results the transition densities and reduced transition probabilities between these QRPA phonons and the QRPA GS defined as their vacuum; this is illustrated by the right plots of Fig. 3.

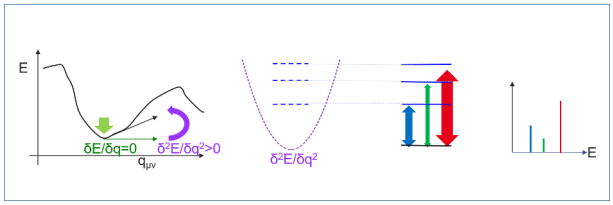

Figure 3. Schematic representation of the linear response applied in QRPA. From left to right, four steps of the QRPA calculation chain: identification of a local minimum, deduced harmonic surface and its eigenmodes, transition probabilities from or to the GS, and discrete QRPA spectrum.

Generally, the discrete spectra are folded with a Lorentzian function to produce PSF, keeping in mind that usually the IV dipole spectrum is the only one to be considered and that many QRPA solvers impose the spherical symmetry. We will discuss in the following sub-section the characteristics of the different PSF models using microscopic ingredients.

3.2.2 From "spherical" Skyrme to the axially deformed "Gogny" via covariant interaction QRPA models

The first large-scale microscopic PSF model proposed in 2002 [20] is based on QRPA calculations on top of HF+BCS[3] using the SLy4 Skyrme interaction. This model

[3]We will not go into the details that differentiate Hartree-Fock-Bogolyubov (HFB) and Hartree-Fock (HF)+BCS, the reader will find the necessary information in books such as [2].

imposes spherical symmetry for all nuclei and, as a second step, splits the entire QRPA strength for deformed nuclei with the recipe given by Eq. (2). In this framework, centroid energies of spherical nuclei are well reproduced and the position of major peak for deformed nuclei are broadly consistent with experimental data. For neutron-rich nuclei, a low-energy pygmy dipole strength is predicted. These results were confirmed by the HFB+QRPA model based on the BSk7 Skyrme interaction published two years later [21]. Within the same formalism where deformation is treated phenomenologically, a dependence on excitation energy is introduced in the RMF-Hartree-Bogolyubov (HB) + QRPA [22], BSk7-HFB+QRPA and BSk27-HFB+ QRPA [23] models (see Table 1) through a phenomenological energy- and temperature-dependent width of the Lorentzian folding the QRPA strength. These approaches provide a good prediction of the centroid energy, including the deformation split, and the appearance of low-energy dipole excitations is also obtained, especially for neutron-rich nuclei. Outside the QRPA framework, there are other models to describe photo-absorption but their scope is limited for now to spherical systems. Among them, one can cite here the quasiparticle phonon model (QPM) with HFB input [24], the ab-initio-based model [25], and the QPM including complex configurations of up to three phonons [26]. Some efforts have also been made from the SM side with work in progress to systematically produce PSF for light spherical and deformed nuclei [27].

In 2018, the first QRPA-based model including an explicit consideration of the intrinsic deformation of the nuclei was implemented on a large scale. Such a model concerns the large-scale application of the Gogny axially symmetric HFB+QRPA approach, previously applied to light systems [28] and upgraded to parallel numerical computing in order to describe multipole vibration of the heavy and deformed ^{238}U isotope [29]. In this method discussed here [30], both electric [5] and magnetic [31] modes have been calculated and included in a microscopic way. Figure 4 shows the dipole split obtained from the axially-symmetric deformed QRPA approach dealing with both angular momentum projection $K = 0$ and $K = 1$ of the dipole mode. We see in Fig. 4 that the large split coincides with a large deformation while nuclei with an almost spherical shape give a negligible split of the peak energy. When the latter is small, it is generally not seen experimentally.

In the D1M+QRPA+0lim model, the upbend low energy component has been analytically estimated from SM calculation. At the same time, high-level excitations and other missing physical ingredients in the QRPA standard approach were emulated by a global energy shift and an adjusted Lorentz folding procedure; for more details on the fit protocol, see Refs. [6, 30].

Furthermore, by comparing the phenomenological model outputs with those based on microscopic approaches, a good reproduction of data was observed for

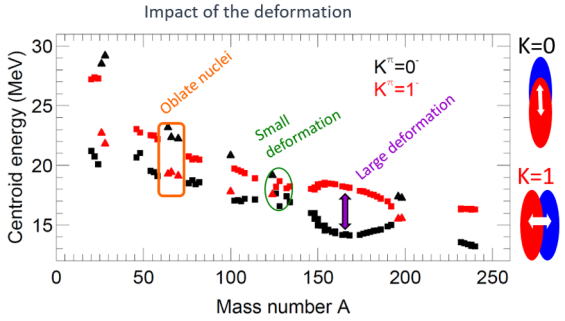

Figure 4. $K = 0$ and $K = 1$ angular momentum projection split of the GDR. Centroid energies of both K components are given as a function of nucleon mass number A for nuclei found intrinsically deformed by the HFB calculation with the D1M Gogny interaction [32]. To facilitate the analysis, the areas of large prolate or oblate deformations as well as very small deformations are indicated on the graph. On the right side are illustrated the two directions of the K-dipole vibration with respect to the symmetry axis or to the perpendicular radius.

the nuclei for which data exist and a better predictability is assumed for the experimentally inaccessible nuclei. This prediction capability is extrapolated from Fig. 5 where the average radiative width $\langle\Gamma_\gamma\rangle$ is plotted as a function of the atomic mass for the three phenomenological above-described Lorentzian models (SLO, GLO and SMLO) and for the aforementioned microscopic model D1M+QRPA+0lim. While the SLO (GLO) predictions overestimate (underestimate) experimental data, both SMLO and D1M+QRPA+0lim are globally in good agreement with data.

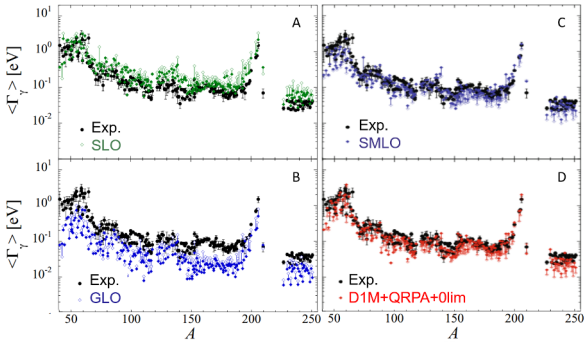

Figure 5. Average radiative width $\langle\Gamma_\gamma\rangle$ as a function of the atomic mass A. Comparison with experimental data [33] with SLO (panel A), GLO (panel B), SMLO (panel C) and D1M+QRPA+0lim (panel D) models. The error bars on theoretical predictions correspond to the use of different nuclear level density models.

3.3 Alternative resolution of the QRPA equations

Now that we have demonstrated the interest in QRPA approaches for the production of PSF, it is pertinent to note

that efforts have been made to produce photo-absorption probability without the full calculation of QRPA matrices and their diagonalization. Such an achievement is possible thanks to the Finite Amplitude Method (FAM) which provides a continuous folded PSF for each multipole transition operator via iterative procedure on top of the HFB solution; for non-iterative Quasi-particle FAM approaches, see Refs. [34, 35] which provide E1 and M1 PSF. Although this QFAM does not provide the phonon wave functions, these can nevertheless be obtained by a supplementary treatment. The performance of this post-processing varies depending on the method used and the number of desired eigenvalues. Another weak point is the smearing value, which is needed to ensure existence of numerical solutions: FAM equations are unsolvable as soon as the energy of the function is equal to an eigenvalue. Each calculation depends on this smearing value and the processing must be started and achieved for each excitation energy and each operator. More details can be found in [36]. Nevertheless, the production of photo-absorption is faster by many order of magnitude than standard matrix resolution. This alternative QRPA resolution is very promising notably for ab-initio approaches [37] or for interaction adjustment protocols that require a good reproduction of the energies of the GR.

3.4 Time dependent mean-field approaches

On the same page, one should mention the recent time-dependent density functional theory (TDDFT) approaches now applied to any deformed nuclei. For example, PSF of the triaxially deformed ^{100}Mo nucleus has been calculated with various Skyrme interactions taking into account the pairing correlations through the BCS formalism [38]. Similar calculations were performed 10 years ago [39, 40] with a normalized pairing field suitable for zero-range interaction as the Skyrme one. In such a framework, the iterative processing is associated to the relaxation of excited nuclei and the multipole mode is extracted via a frequency decomposition. These approaches are illustrated schematically in Fig. 2, where the periods of pure vibration modes are indicated by arrows. This theoretical framework is very promising even if it is limited today to the electric modes. For future developments, mention should be made of recent work on quantum fluctuations inducing collective multiphonons using an extension of the nuclear time-dependent density-functional theory [41].

4 Photo-absorption versus γ-decay, what's new?

As suggested above, the more microscopic the nuclear structure and reaction models are, the more accurate and reliable the databases generated with them will be. It is therefore legitimate to ask which other improvements or developments of the microscopic models are both feasible and relevant for future PSF modelling. It is now time to introduce different calculation chains for the assessment of the probabilities of photo-absorption or γ-decay probabilities. The main point of previous evaluations was based on the reciprocity between the probability of absorbing a photon and that of emitting it by inverting the initial and final states. But, if the absorption of a photon is a process that transforms the GS of a nucleus into all dipolar states (we recall here that the transitions E1 and M1 are dominant), the decay process itself occurs for many different spin and parity states that do not only de-excite on the GS. The reciprocity is pertinent only if the initial state for absorption is a single one (GS for example) and the photon emission lands to a unique final state, ideally the same GS. The picture given in Fig. 6 illustrates this reciprocity.

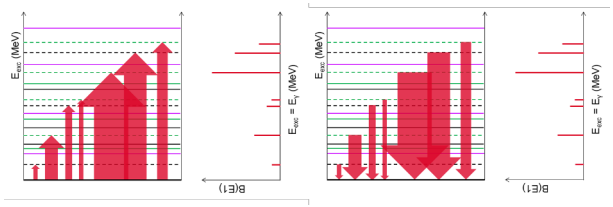

Figure 6. Reciprocity between absorption from the GS and decay to the GS. The width of the arrows are proportional to the transition probabilities, hence proportional the height of the discrete QRPA spectrum.

On the other hand, the decay scheme of Fig. 7 shows that it is necessary to evaluate the transitions between all phonons described by the underlying microscopic model, whatever it may be. Fortunately, it is now possible to calculate these quantities for the QRPA phonons. Indeed, the explicit calculation of transitions between the QRPA solutions was implemented to include a Coriolis mixing on isomeric state description [42]. This upgrade of the QRPA post-processing can be now used also for other application as the γ cascade.

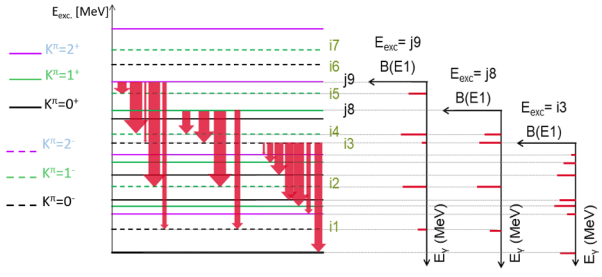

Figure 7. Illustration of the discrete spectra obtained for different initial states (excited ones) decaying to all accessible state by E1 down to the GS if spin and parity rules are fulfilled. The K and parity are given in the legend. The GS is imposed to be $J^\pi = 0^+$ for simplicity and related to the GS properties of almost all even-even nuclei.

For deformed nuclei one should keep in mind that rotational states with $J \geq |K|$ are involved. The method of

constructing rotational states is the same as that used in QRPA level density calculations [43]. Intrinsic transitions for band head should then be calculated and some geometrical formulas used to extract reduced transition matrix elements. The calculation of the reduced matrix elements must be carried out within a rotation band or between two states belonging to two different bands for which the values of K differ by no more than 1 unit value and for which the parity is the same (magnetic case) or opposite (electric case). The first type of transitions are called intra-band transitions, they are obtained through dipole moment of each QRPA phonon. The second type of transition are inter-band ones, their evaluation needs the explicit calculation of dipole operator from one QRPA initial state to another final QRPA one. To generate all the M1 and E1 decay transitions, inter-band and intra-band, one should in principle generate all the QRPA states for $J = 0$ up to the maximum spin value J_{max} accessible for the compound nucleus. This means that QRPA calculations are needed for all K blocks with $K = 0, .., J_{max}$. In the following example, we have calculated the phonons QRPA for values of K up to 9. The quantity which is plotted in Fig. 8 is close to the PSF definition for γ-decay, omitting transitions down to the GS (these latter quantity is already a solution of the standard QRPA approach). The link between PSFs shown in Fig. 8 and the absorption probability needs more adjustments to insure the reciprocity of emitting/absorbing a gamma to, or from, the GS. In other words, the final PSF is a more elaborate form of the present quantity, but its behaviour, in particular the low-energy M1 upbend which appears here (lower panel of Fig. 8) will be reflected into the PSF. These preliminary results show how more microscopic ingredients can be included in the description of the PSF; their impact will be soon analyzed.

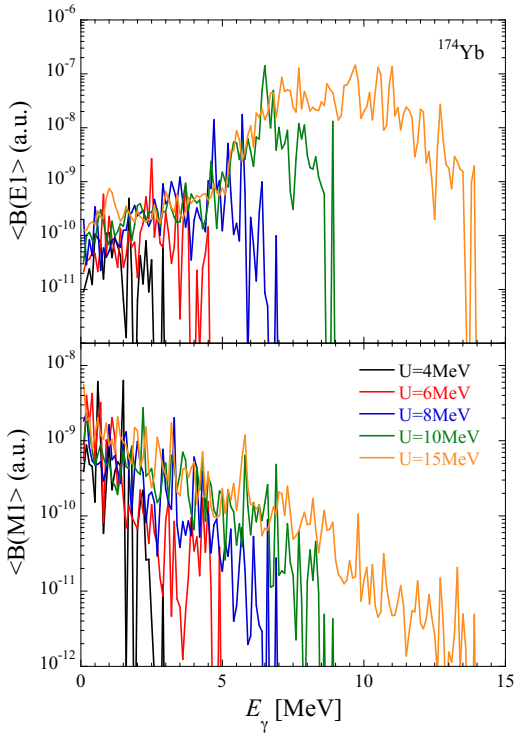

Figure 8. Averaged values of $B(\mathrm{M1},E_\gamma)$ and $B(\mathrm{E1},E_\gamma)$ for various excitation energies U. The average is made for intervals of 100keV.

5 Conclusions and prospects

Although the PSF is not an observable, it remains an essential ingredient of nuclear databases in particular for reaction cross section calculations. Its extraction by convolution or deconvolution of experimental observables remains delicate even for nuclei accessible by experiment. In addition, its evaluation is necessary for many processes and needs to be applied for almost all nuclear systems that can be bound. Although purely phenomenological models are still popular and widely used, they coexist with increasingly microscopic-based approaches that compete with them. As seen over the past decade, the inclusion of microscopic ingredients significantly improves the γ-ray strength function models.

Today, we want PSF models that can be extended to the entire nuclear chart. To do this, the HFB+QRPA microscopic approach is by far the most popular candidate because it can be applied a priori to all nuclei with equal confidence. Indeed, many models of photo-absorption PSF based on QRPA have been obtained for various interactions. It should be borne in mind that approaches beyond QRPA are promising, especially the QPM and ab initio approaches and results of the modern SM is also competitive for light systems. The TDDFT can also provide photo-absorption PSF for many systems up to the heaviest including deformed nuclei. The probabilities of intra-band and inter-band transitions are now available beyond the standard use of QRPA results. Work is underway to further develop PSF models with microscopic inputs. The PSF will depend not only on the energy of the photon but also on the excitation energy, and also on the spin and parity of the states considered. These quantities are easily accessible from microscopic models such as QRPA and its extensions.

References

[1] A. J. Koning, S. Hilaire, S. Goriely, Eur. Phys. J. A **59**, 131 (2023); A. J. Koning, S. Hilaire, S. Goriely, Erratum Eur. Phys. J. A **59**, 146 (2023) 10.1140/epja/s10050-023-01034-3

[2] P. Ring, P. Schuck, *The Nuclear Many-Body Problem*, (Springer, 2004).

[3] M.N. Harakeh and A. van der Woude. *Giant Resonances: Fundamental high-frequency modes of nuclear excitation*, (Oxford Science Publications, 2001).

[4] J. Dechargé, L. Sips, Nucl. Phys. A **407**, 1 (1983). 10.1016/0375-9474(83)90305-6

[5] M. Martini, S. Péru, S. Hilaire et al., Phys. Rev. C **94**, 014304 (2016). 10.1103/PhysRevC.94.014304
[6] S. Goriely, P. Dimitriou, M. Wiedeking et al., Eur. Phys. J. A **55**, 172 (2019). 10.1140/epja/i2019-12840-1
[7] P. Axel, Phys. Rev. **126**, 671 (1962). 10.1103/PhysRev.126.671
[8] J. Kopecky, M. Uhl, Phys. Rev. C **41**, 1941(1990). 10.1103/PhysRevC.41.1941
[9] S. Goriely, Phys. Lett. B **436**,10 (1998). 10.1016/S0370-2693(98)00907-1
[10] S.G. Kadmenskii, V.P. Markushev, V.I. Furmann, Sov. J. Nucl. Phys. **37**,165 (1983).
[11] F.-K. Thielemann, M. Arnould, in: K. Böckhoff (Ed.), Proceedings of Conference on Nuclear Data for Science and Technology, Reidel, Dordrecht, p. 762 (1983).
[12] V.A. Plujko, O.M. Gorbachenko, R.Capote, P. Dimitriou, At. Data Nucl. Data Tables **123**, 1 (2018). 10.1016/j.adt.2018.03.002
[13] S. Goriely, V. Plujko, Phys. Rev. C **99**, 014303 (2019). 10.1103/PhysRevC.99.014303
[14] A. Voinov, E. Algin, U. Agvaanluvsan et al., Phys. Rev. Lett. **93**, 142504 (2004). 10.1103/PhysRevLett.93.142504
[15] M. Guttormsen, R. Chankova1, U. Agvaanluvsan et al., Phys. Rev. C **71**, 044307 (2005). 10.1103/PhysRevC.71.044307
[16] K. Sieja, Phys. Rev. Lett. **119**, 052502 (2017). 10.1103/PhysRevLett.119.052502
[17] R. Schwengner, S. Frauendorf, B. A. Brown, Phys. Rev. Lett. **118**, 092502 (2017). 10.1103/PhysRevLett.118.092502
[18] J. E. Midtbø, A. C. Larsen, T. Renstrøm et al., Phys. Rev. C **98**, 064321 (2018). 10.1103/PhysRevC.98.064321
[19] S. Péru, M. Martini, Eur. Phys. J. A **50**, 88 (2014). 10.1140/epja/i2014-14088-7
[20] S. Goriely, E. Khan, Nucl. Phys. A **706**, 217 (2002). 10.1016/S0375-9474(02)00860-6
[21] S. Goriely, E. Khan, M. Samyn, Nucl. Phys. A **739**, 331 (2004). 10.1016/j.nuclphysa.2004.04.105
[22] I. Daoutidis, S. Goriely, Phys. Rev. C **86**, 034328 (2012).10.1103/PhysRevC.86.034328
[23] Y. Xu, S. Goriely, E. Khan, Phys. Rev. C **104**, 044301 (2021). 10.1103/PhysRevC.104.044301
[24] N. Tsoneva, H. Lenske, Ch. Stoyanov, Phys. Lett. B **586**, 213 (2004). 10.1016/j.physletb.2004.02.024
[25] M. Markova, A. C. Larsen, P. von Neumann-Cosel et al., Phys. Rev. C **109**, 054311 (2024). 10.1103/PhysRevC.109.054311
[26] D. Savran, M. Elvers, J. Endres et al., Phys. Rev. C **84**, 024326 (2011). 10.1103/PhysRevC.84.024326
[27] O. Le Noan, K. Sieja, *Electric dipole response of sd-shell nuclei within the Large-Scale Shell Model approach*, 9th Workshop on Level Density and Gamma Strength, Oslo (2024).
[28] S. Péru, H. Goutte, Phys. Rev. C **77**, 044313 (2008). 10.1103/PhysRevC.77.044313
[29] S. Péru, G. Gosselin, M. Martiniet al., Phys. Rev. C **83**, 014314 (2011). 10.1103/PhysRevC.83.014314
[30] S. Goriely, S. Hilaire, S. Péru, K. Sieja, Phys. Rev. C **98**, 014327 (2018). 10.1103/PhysRevC.98.014327
[31] S. Goriely, S. Hilaire, S. Péru et al., Phys. Rev. C **94**, 044306 (2016). 10.1103/PhysRevC.94.044306
[32] S. Goriely, S. Hilaire, M. Girod, S. Péru, Phys. Rev. Lett. **102**, 242501, (2009). 10.1103/PhysRevLett.102.242501
[33] R. Capote, M.Herman, P. Oblozinsky et al., Nucl. Data Sheets **110**, 3107 (2009). 10.1016/j.nds.2009.10.004
[34] H. Sasaki, T. Kawano, I. Stetcu, Phys. Rev. C **105**, 044311 (2022). 10.1103/PhysRevC.105.044311
[35] H. Sasaki, T. Kawano, and I. Stetcu, Phys. Rev. C **107**, 054312 (2023). 10.1103/PhysRevC.107.054312
[36] F. Mercier, J.-P. Ebran, E. Khan, Phys. Rev. C **105**, 034343 (2022). 10.1103/PhysRevC.105.034343
[37] Y. Beaujeault-Taudière, M. Frosini, J.-P. Ebran et al., Phys. Rev. C **107**, L021302 (2023). 10.1103/PhysRevC.107.L021302
[38] Yue Shi, P. D. Stevenson, Chinese Physics C **47**, 034105 (2023). 10.1088/1674-1137/acac6b
[39] I. Stetcu, A. Bulgac, P. Magierski, K. J. Roche, Phys. Rev. C **84**, 051309R (2011). 10.1103/PhysRevC.84.051309
[40] I. Stetcu, C.A. Bertulani, A. Bulga et al., Phys. Rev. Lett. **114**, 012701 (2015). 10.1103/PhysRevLett.114.012701
[41] P. Marević, D. Regnier, D. Lacroix, Phys. Rev. C **108**, 014620 (2023).10.1103/PhysRevC.108.014620
[42] L. Gaudefroy, S. Péru, N. Arnal et al., Phys. Rev. C **97**, 064317 (2018). 10.1103/PhysRevC.97.064317
[43] S. Hilaire, S. Goriely, S. Péru, G. Gosselin, Phys. Lett. B **843** 137989, (2023). 10.1016/j.physletb.2023.137989